PREPARATION AND CHARACTERIZATION OF BARIUM HEXAFERRITE BY BARIUM MONOFERRITE

A dissertation submitted
in the partial fulfilment of the
award of Degree of

Master of Technology
In
MATERIALS AND METALLURGICAL ENGINEERING

Submitted By:
POOJA CHAUHAN
Roll No - 600802014

Under the supervision of
Dr. PUNEET SHARMA
Assistant Professor
School of Physics & Material Science
Thapar University
Patiala – 147004
2010

CERTIFICATE

I hereby declare that the report entitled **"PREPARATION AND CHARACTERIZATION OF BARIUM HEXAFERRITE FROM BARIUM MONOFERRITE"** is an authentic record of my own work carried out as requirements for the award of degree of M. Tech. (Materials & Metallurgical Engineering) at Thapar University, Patiala, under the guidance of Dr. Puneet Sharma (SPMS) during January to June 2010.The matter presented in this thesis has not been submitted in part or full to any other University or Institute for the award of any degree.

Pooja Chauhan

Date: 15.07.10

Pooja Chauhan

Roll No: 600802014

It is certified that the above statement made by the candidate is correct to best of my knowledge and belief.

15/7/10

Dr. Puneet Sharma

Assistant Professor

School of Physics and Materials Science

Thapar University, Patiala- 140074

Countersigned by:

Dr. O.P. Pandey

Professor & Head (SPMS)

Thapar University

Patiala-140074

21.7.10

Dr. R. K. Sharma

Dean, Acadmic Affairs

Thapar University

Patiala-140074

ACKNOWELEDGMENT

I would like to thanks Dr. Puneet Sharma, Assistant Professor (SPMS), giving me a chance to work in their supervision and without whose help and constant guidance this thesis would have not taken shape. I am extremely thankful to Dr. O. P. Pandey, Head, SPMS for their cooperation and encouragement. I am also thankful to Mr. Purshottam and all staff of SPMS, for their constant cooperation in the technical and experimental work.

I am highly grateful to my friend Mr. Deepak Kumar who provided their valuable guidance and suggestions during the course of the work. I acknowledge with thanks for encouragement of my elders and relatives. I am very thankful to my parents for their constant co-operation, inspiration, patience, blessing and moral support.

Pooja Chauhan
(600802014)

Dedicated

to my

parents

CONTENTS

LIST OF FIGURE

LIST OF TABLE

CHAPTER-1 Page No.

CHAPTER-4

Chapter 1

Introduction

Introduction

Overview

This Chapter reviews the basic concepts of permanent magnetic materials and importance on M-type ferrite particularly barium ferrite permanent magnets. M-type ferrites are compared with other important permanent magnets and their historical development is described. The crystal structure, magnetic structure and phase relationship of barium ferrite are outlined. The intrinsic magnetic properties of M-type ferrite are presented in detail. An account of the various processing techniques used for manufacturing. The properties of commercial barium ferrite permanent magnets and applications are illustrated. The aim of the work is given in the end of this chapter.

1.1 Magnetic materials

Magnetic materials can be divided into two group soft and hard magnetic materials. The soft magnetic materials are those materials which are magnetized and demagnetized easily while the hard magnetic materials are those which are difficult to magnetize and demagnetize.

The hard magnetic materials have high coercivity, because the high coercivity resists the magnetization action. The basic difference of two types of permanent magnets was described on the basis of hysteresis loop. The soft magnetic materials exhibit a narrow hysteresis loop, whereas; the hard magnetic materials show a broad hysteresis loop. In the narrow hysteresis loop magnetization follows the variation of the applied field without significant loss. The broad hysteresis loop shows the magnetic energy that can be stored in the materials [1].

1.2 Soft magnetic materials

Soft magnetic materials can be easily magnetized and demagnetized. They retain their magnetization only in presence of a magnetic field. They show a narrow hysteresis loop, so that the magnetization follows the variation of applied field nearly without hysteresis loss [2]. They are used to enhance the flux, produced by an electric current in them. The quality factor of a soft magnetic material is to measure of its permeability with respect to the applied magnetic field. The other main parameter is the corecivity, saturation magnetization and the electrical conductivity. An ideal soft magnetic material would have low coericivty (H_c), a very large saturation magnetization (M_s), zero remanence (B_r), zero hysteresis loss and very large permeability [3]. The hysteresis loop of soft magnetic material is shown in figure 1.1

[4]. Few important soft magnetic materials are Fe, Fe-Si alloys, soft ferrites ($MnZnFe_2O_4$), silicon iron etc.

1.3 Hard magnetic materials

Hard Magnetic materials also called as permanent magnets are used to produce strong field without applying a current to coil. Permanent magnets required high coercivity, so they should exhibit a strong net magnetization and is stable in the presence of external fields, which requires high coercivity. In hard magnetic materials uniaxial magnetic anisotropy is necessary and the following magnetic properties are required [5]. Important properties of hard magnetic materials are mentioned below:

High coercivity: The coercivity, also called the coercive field, of a ferromagnetic material is the intensity of the applied magnetic field required to reduce the magnetization of that material to zero after the magnetization of the sample has been driven to saturation. Coercivity is usually measured in oersted or ampere/meter units and is denoted H_c. Materials with high coercivity are called hard ferromagnetic materials, and are used to make permanent magnets [6].

Large magnetization: The process of making a substance temporarily or permanently magnetic, as by insertion the material in a magnetic field.

Rectangular hysteresis loop: A hysteresis loop shows the relationship between the induced magnetic flux density (B) and the magnetizing force (H). hard magnetic materials have rectangular hysteresis loop [7].

Hard magnetic material has the wide hysteresis loop due to strong magnetization which is shown in figure 1.1.

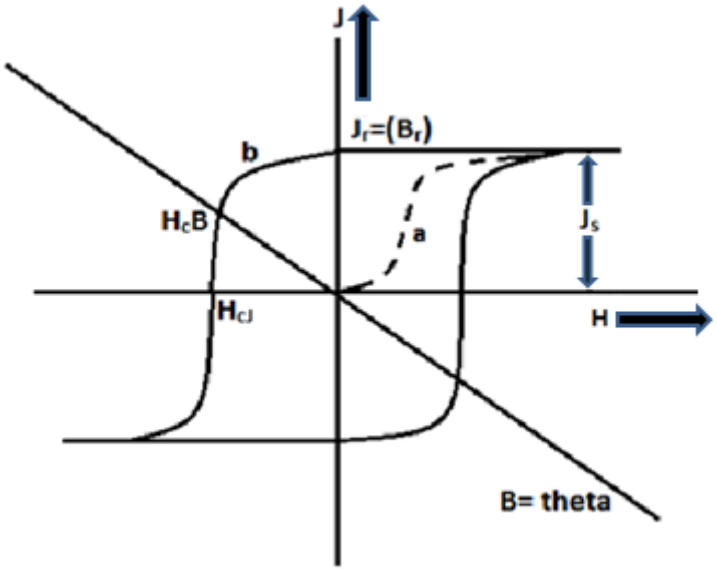

Figure 1.1 Hysteresis loop for hard magnetic materials

1.4 Classification of hard magnetic materials

Among the permanent magnetic materials the important materials are alnico, hard ferrite, samarium cobalt and neodymium-iron-boron. Each of these materials exhibits different set of properties. By comparison with production cost, the hard ferrites found to be the most suitable. A comparison of commercial permanent magnets in terms of magnetic properties, temperature coefficient of remanence and coercivity, temperature behavior, availability of raw materials with their relative cost which is given in Table 1.1. By comparing the cost of different materials it is found that ferrites are most economical. The comparison shows that rare earth based magnets have better magnetic properties as compared to ferrite [8].

Table 1.1 Comparison of commercial permanent magnetic materials [8]

Parameter	**Ferrite**	**Alnico**	**$SmCO_5$**	**Nd-Fe-B**
B_r (mT)	370	700-1200	890	1100
H_{ci} (kA/m)	255	50-150	1200	>1000
$(BH)_{max}(kJ/m^3)$	30	60-80	150	350
T_c (K)	750	860	933	585
α ($\%K^{-1}$)	-0.20	-0.02	-0.05	-0.13
β ($\%K^{-1}$)	+0.40	-0.03	-0.03	-0.60
Max. Operation Temperature(K)	523	773	523	373
Raw material source	Very good	Poor	Poor	Good
Density(kg/m^3)	4650	7300	8300	7400
Price ratio/ magnetic energy	1	7.5	23	7

Among the class of hard magnetic materials the hard ferrite are very important due to its moderate magnetic properties at lower cost. The following section will emphasis on hard ferrites.

1.5 Hard ferrites

The term ferrite is commonly used generically to describe a class of magnetic oxide compounds, which contains iron oxide as a principal component. Magnetite, Fe_3O_4 also called loadstone, is a genuine ferrite and also was the first magnetic materials known to the ancient people. Ferrites can be classified according to crystal structure, i.e. cubic vs. hexagonal ferrite, or magnetic behavior, i.e. soft vs. hard ferrite. Soft ferrites are easy to magnetize and demagnetize. Hard ferrites are hard to magnetize and demagnetize. Hard magnetic materials are commonly used for permanent magnetic applications. Hard ferrites have a hexagonal structure and can be classified as M-, W-, X-, Y-, Z- type ferrites [8]. Table 1.2 shows the types of ferrites and their respective chemical formulae.

Table 1.2 A comparison of the Hard Ferrites [8-9-10]

Types	**Chemical Formula**	
M-	$RFe_{12}O_{19}$	R = Ba, Sr, Pb
W-	RMe_2Fe_{16}	Me = Fe^{+2}, Ni^{+2}, Mn^{+2} etc
X-	$RMeFe_{28}$	
Y-	$R_2Me_2Fe_{12}O_{22}$	
Z-	$R_3Me_2Fe_{12}O_{41}$	

W-, X-, Y-, Z- type are not important economically because of their relatively difficult processing. The chemical composition of various hexagonal compounds is shown in the fig.1.2 [11], as part of ternary phase diagram for BaO-MeO-Fe_2O_3 system. Here MeO represents a divalent ion among the first transition elements, Zn,

Mg or a combination of ions whose valencey is two. S denotes a cubic spinel $MeO.Fe_2O_3$.

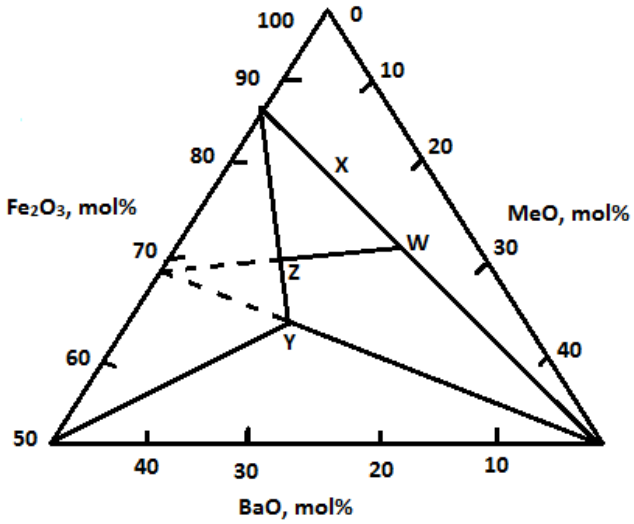

Figure 1.2 Compositional phase diagram for hexagonal ferrites

1.6 M-Type ferrites

M-type ferrites with the formulae of $BaO.6Fe_2O_3$ (BaM), $SrO.6Fe_2O_3$ (SrM) and $PbO.6Fe_2O_3$ (PbM) are by far the most important hexagonal ferrites. M-type ferrites are mainly used as permanent magnet materials that have strong resistance to demagnetizing field once they get magnetized and have a dominant position in permanent magnet market. They are preferred over alnicos due to lower material and processing cost and superior coercivity. Sr-Ferrite and Ba-Ferrite are the two main materials in the M-type ferrite family. These ferrites have moderate magnetic properties, and price per unit of available magnetic energy is very less.

1.7 Crystal structure, magnetic structure and phase diagram of M-Type ferrites

The crystal structure of M-type ferrites was determined by Adelskold. Figure1.3 shows the unit cell of barium hexaferrite [12]. The crystal structure consists of two formula units. Its symmetry is characterized by the space group P63/*mmc*. In the unit cell, the O^{-2} ions form a hexagonal close packed lattice. Every five oxygen layers, one O^{-2} ion is replaced with Ba due to the similarity of their ionic radii. The structure is build up from smaller unit: a cubic block S, having the spinal structure and a hexagonal block R, containing Sr^{+2} ions [12-13]. Five oxygen layers make one molecule and two molecules make one unit cell. Each molecule shows 180 degree rotational symmetry around the hexagonal *c*-axis against the lower or upper molecule. The O^{-2} layer containing Ba^{+2} is a mirror plane being perpendicular to the *c*-axis. Fe^{+3} ions occupy interstitial positions at different crystallographic sites i.e. tetrahedral, octahedral and hexahedral sites of oxygen lattice.

On the other hand, if we consider the magnetic concept, then found that, M-type compounds have a typical ferrimagnetic structure. The magnetism of $BaFe_{12}O_{19}$ comes from the ferric iron, each carrying a magnetic moment of $5\mu_B$. These are aligned to give either parallel or anti parallel ferromagnetic interaction. Ions of the same crystallographic position are aligned parallel which constitute a magnetic sub lattice. The interaction between neighbouring ions of different sub lattice is a result of super exchange by oxygen ion. The theory predicts that the atomic moments are parallel when Fe-O-Fe angle is about 180 degree and anti parallel when this angle is about 90 degree [13]. In figure 1.3 S block contains four Fe^{+3} of up spin in octahedral sites and two Fe^{+3} of down spin in tetrahedral site [14]. In R block there exist three

Fe^{+3} of up spin in octahedral site, two Fe^{+3} of down spin in octahedral sites and one Fe^{+3} of up spin in trigonal bipyramid site [11]. The exchange scheme of the compound is shown in figure 1.3. Table 1.3 shows the crystallographic properties of the M-Type ferrites [1].

Table 1.3 Crystallographic properties of M-type ferrites

Parameter		**Ferrite (S)**		
Lattice Constant (nm)	**a**	**BaM**	**SrM**	**PbM**
		0.5893	0.588	0.588
	c	2.3194	2.307	2.302
Molecular Weight		1112	1062	1181
Density gm/cc		5.28	5.11	5.68

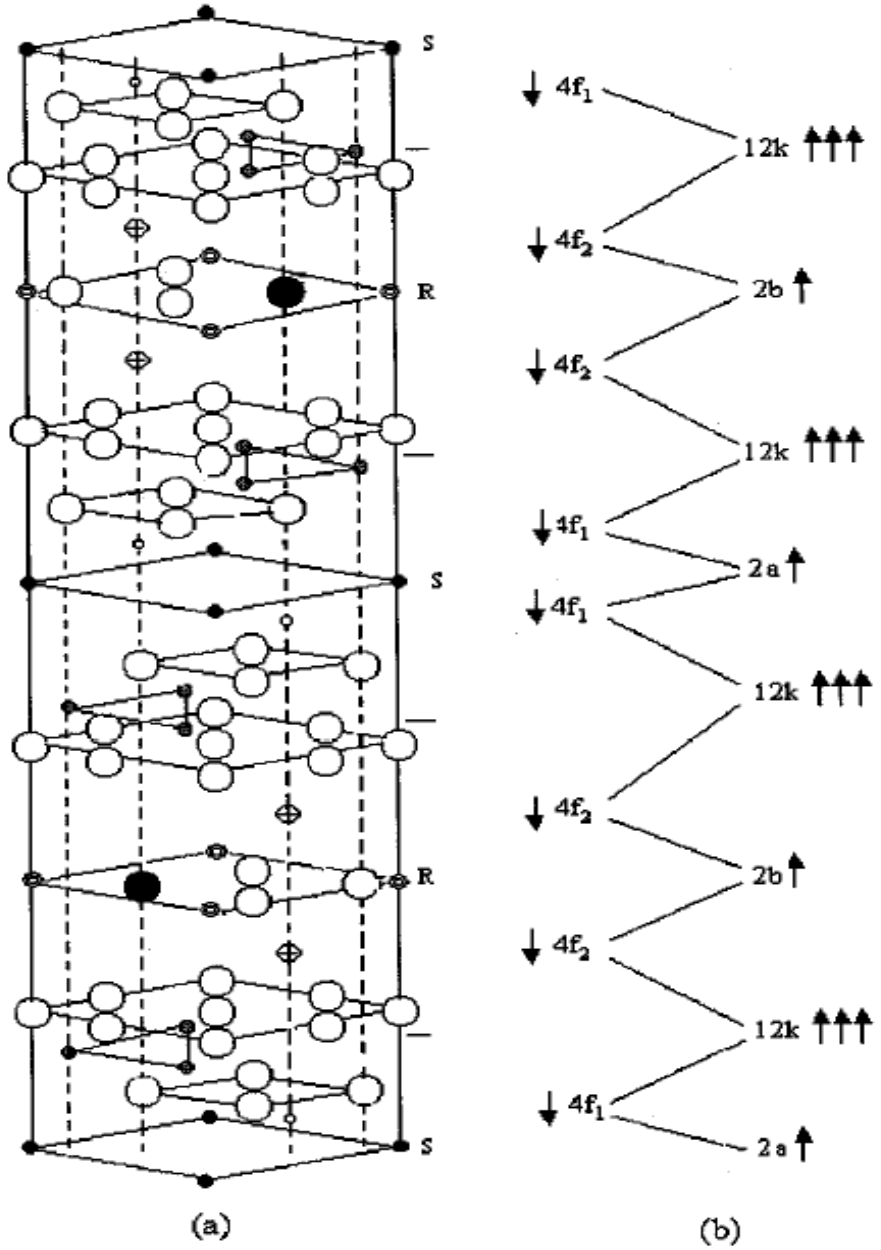

Figure 1.3 (a) Crystal structure and (b) Magnetic structure

M-type (a) Crystal structure showing the S and R subunits where ○ is O^{2-}; ● is Sr^{2+}; ■, ◈, ●, ⭘, and all Fe^{3+} at $4f_1$, 2b, 12k, $4f_2$, and 2a positions respectively. (b) Magnetic structure where the arrows represent size and spin direction of unpaired electron at various crystallographic positions.

The total magnetization at temperature T therefore can be expressed as:

$$\mathbf{Js\ (T) = 6\sigma_k\ (T) - 2\sigma_{f1}\ (T) - 2\sigma_{f2}\ (T) + \sigma_b\ (T) + \sigma_a\ (T)}$$

Where σ_k , σ_{f1} , σ_{f2} , σ_b , and σ_a represents the magnetization of one Fe^{+3} ion in each sub lattice. Because Fe^{+3} has a magnetic moment of $5\mu_B$ at 0K so that the net magnetic moment calculated at 0K is $20\mu_B$ for each unit cell.

Table 1.4 Summary of the crystal structure and magnetic structure

Sub lattice	**Co-ordination**	**Number of ions**	**Spin**
12K	Octahedral	6	Up
$4f_1$	Tetrahedral	2	Down
$4f_2$	Octahedral	2	Down
2a	Octahedral	1	Up
2b	Fivefold (Trigonal bi-pyramind)	1	Up

Figure 1.4 shows the phase diagram of BaO and Fe_2O_3 system. In the phase diagram the homogeneity range is very narrow and in the eutectic range somewhat enlarged, at most towards the side rich in the BaO [15].

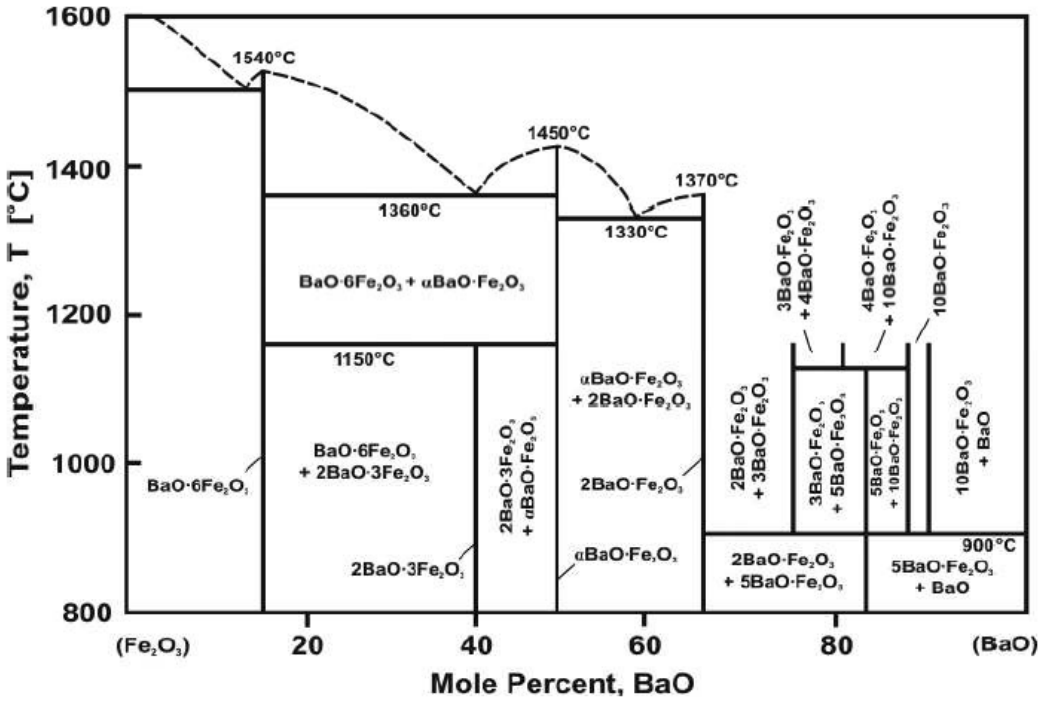

Figure 1.4 Phase diagram of Fe_2O_3-BaO system

Towards higher temperature range, incongruent melting occurs at 1448 ^{0}C (1 bar O_2) and 1390 ^{0}C (air), with the W phase $BaFe_{18}O_{27}$ (= BaO 2FeO.8Fe_2O_3) is formed [13]. However, in vacuum annealing above 1100 ^{0}C, Fe_3O_4 and S7F5 phase is formed with the release of oxygen, where S= 2(BaO.Fe_2O_3) and F= BaO. 6Fe_2O_3 or $BaFe_{12}O_{19}$ phase is stable only towards lower temperature range. Towards the Fe_2O_3 richer side the two phase region ($BaFe_{12}O_{19}$ + Fe_2O_3) are formed. On the BaO richer region, the phase S7F5 and S3F2 are the neighbouring phases both of them being very close to the composition S4F3 [16]. The eutectic temperatures of 1210 ^{0}C (1 bar O_2) or 1195 ^{0}C (air) as well as the eutectic content of 53.5 or 55 mole % are close to one another.

1.8 Intrinsic magnetic properties of M-Type ferrites

The intrinsic magnetic properties are subdivided into primary and secondary one. The primary properties such as saturation magnetization *Js* and magneto crystalline anisotropy constant *K1* are directly related to the magnetic structure. The secondary magnetic properties such as anisotropy field strength H_A and the specific domain wall energy (γ_w) are derived from the primary ones. The secondary magnetic properties characterize the actual magnetic state. These govern the actual magnetic behavior. The primary and secondary magnetic properties characterize the actual magnetic state. These govern the actual magnetic behavior. The primary and secondary magnetic properties are shown in table 1.5 [1].

Table 1.5 Primary and secondary properties of M-Type ferrites

Primary Properties	
Saturation Magnetization, mT	475
Anisotropic constant, kJ/m^3	360
Curie temperature, K	750
Secondary Properties	
Specific wall energy, J/m^2	54.2×10^{-4}
Anisotropy Field H_A, kA/m	1506
Max Coercivity, $(H_c)_{max}$	1240

The saturation magnetization, *Js* is the maximum magnetic moment per unit volume per gram. It is easily derived from the spin configuration of the sub-lattices, eight ionic moments and $40\mu_B$ per unit cell, which corresponds to 668 mT at 0K [11].

1.9 Processing methods

There are various type of method to process hard ferrites which can classify in major three types:

1. Solid state synthesis method
2. Chemical Co-precipitation methods
3. High energy ball milling method

1.9.1 High Energy Ball Milling (HEBM)

Ball mill is a good tool for grinding many materials into fine powder. The Ball Mill is used to grind many kinds of mine and other materials. There are two type of grinding: the dry process and the wet process. It can be divided into tabular type and flowing type according to different forms of discharging material. After the grinding the state of the solid is changed: the size and shape of grain etc.

Ball mill is horizontal type and tubular running device has two warehouses. This machine is grid type and its outside runs along gear. The material enters spirally and evenly the first warehouse of the milling machine along the input material hollow axis by input material device. In this warehouse, there is a ladder scaleboard or ripple scaleboard, and different specification steel balls are installed on the scaleboard, when the barrel body rotates and then produces centrifugal force ,at this time , the steel ball is carried to some height and falls to make the material grinding and striking. After grinded coarsely in the first warehouse, the material then enters into the second warehouse for regrinding with the steel ball and scaleboard. In the end, the powder is discharged by output material board and the end products are completed.

The ball mill is a key equipment for grinding. It is widely used for the cement, the silicate product, new type building material, fire-proof material, chemical fertilizer, black and non-ferrous metal, glass, ceramics and etc. Ball mill can grind ore or other materials that can be grinded either by wet process or by dry process [17].

Benefits of ball mill

- Increase of the surface area of a solid
- Manufacturing of a solid with a desired grain size
- Pulping of resources

1.9.2 Chemical Co-precipitation

Co-precipitation (CPT) is carrying down by a precipitate of substances normally soluble under the conditions employed. In medicine, co-precipitation is specifically the precipitation of an unbound "antigen along with an antigen-antibody complex". There are three main mechanisms of co-precipitation: inclusion, occlusion, and adsorption [18]. An inclusion occurs when the impurity occupies a lattice site in the crystal structure of the carrier, resulting in a crystallographic defect, this can happen when the ionic radius and charge of the impurity are similar to those of the carrier. An adsorbate is an impurity that is weakly bound (adsorbed) to the surface of the precipitate. An occlusion occurs when an adsorbed impurity gets physically trapped inside the crystal as it grows [19].

1.9.3 Sol-gel method

In this method, the 'sol' gradually evolves towards the formation of a gel-like diphase system containing both a liquid phase and solid phase whose morphologies range

from discrete particles to continuous particles. In the case of the colloid, the volume fraction or density of particles may low that a significant amount of fluid may need to be removed initially for the gel-like properties to be recognized [20]. To removing of the remaining liquid phase apply a drying process. The rate at which the solvent can be removed is ultimately determined by the distribution of porosity in the gel. The microstructure of the final component will clearly be strongly influenced by changes imposed upon the structural template during this phase of processing. After this, a thermal treatment or firing process is necessary for further polycondensation. When we do the final sintering, we found enhance mechanical properties, structural stability, densification and grain growth [21].

The sol-gel technique is a cheap and low-temperature technique that allows for the fine control of the product's chemical composition. Sol-gel derived materials have diverse applications in optics, electronics, energy, space etc [22].

1.9.4 Solid state reaction method

Among the various processing method solid state synthesis is widely used. The solid solid state synthesis is basically a diffusion method. This method starts with mixing of of barium carbonate and iron cloride to homogenize the raw materials, and can take place either with a wet or dry process. In wet mixing, generally using an aqueous suspension, vibration drum or agitator mills are used. This mixing method is extremely effective but requires energy for dewatering and drying. For this purpose, the suspension can be dewatered either mechanically, e.g., in a filter press and then dried. Dry mixing is done either by grinding and mixing in drum or ball mills or intensive mixing in an edge runner mill or in high intensity counter flow mixer with swirler. The first method is used when the raw materials are not fine enough for the

subsequent reaction. Using second method, the materials can be fed directly to the reaction furnace.

Calcination facilitates solid state diffusion of BaO and Fe_2O_3 and converts the raw materials into the hexaferrite phase. The total reaction C to form strontium ferrite phase takes place in the two unit steps A and B [23]:

A: $BaCO_3 + Fe_2O_3 \longrightarrow BaO.Fe_2O_3 + CO_2$

B: $BaO.Fe_2O_3 + 5Fe_2O_3 \longrightarrow BaO.6Fe_2O_3$

C: $BaCO_3 + 6Fe_2O_3 \longrightarrow BaO.6Fe_2O_3 + CO_2$

The intermediate product, which occurs, is the monoferrite $BaO.Fe_2O_3$.

The calcination temperature also plays an important role in the formation of hexaferrite phase. If the calcination temperature is low, then grains of uniform BaM are not formed. Similarly, if the calcination temperature is too high, excessive grain growth occurs and coarse grain BaM is formed. An optimum temperature for calcination is decided based on silica content in Fe_2O_3 powder.

1.10 Applications of the hard ferrites

Owing to its low price, ferrite magnets are used for a number of applications ranging from magnetic holding tools to motors and generators. The ferrites have replaced other magnet materials in the existing systems, either with or without modification to the system. This is particularly the case with static applications where small demagnetizing fields are involved. A typical example is the application of flat ring instead of high metallic center core magnets in loudspeaker systems. The high H_c has

stimulated the development of the new system, especially in the dynamic application where periodically high demagnetizing fields are present. A typical example is the electric motor with its strong armature electric field. New electric motors are being developed which require very high H_{cj} value lying far beyond the range of Al-Ni-Co materials, for example the starter motor, requiring $H_{cj} > 320$ kA/m.

Applications of hard ferrite other than permanent magnets are in the field of microwave, magnetic bubble memories, magnetic tape recording and magneto-optics. M-type ferrites are of interest for resonance type microwave devices e.g. isolators, filters, and circulators. Below 20 GHz, such devices normally employ garnet or spinel ferrite in combination with the bias magnets. At high frequencies the required bias field becomes impracticably high (>570 kA/m). M-type ferrites are then preferred because of their large anisotropic field,which act as built-in bias field and provides a resonance frequency of about 50 GHz in a small tuning field. For broader frequency coverage, various substitutions can be employed by which H_A is altered. Other, application of magnets in magneto-therapy, purification, magnetic bearing, and automatic camera are a few more applications, which are increasingly becoming important. Some of the common applications in device used in everyday life are highlighted in table 1.6 [1].

Table 1.6 Common application of BaM ferrites

Devices	Parts
Cassette recorder	Speaker, synchronous motor, mike etc.
Video cassette recorder	Main wheel motor
TV sets	Speaker, color adjusting magnet
Air conditioner	Fan motor
Refrigerator	Fan motor, compressor motor, rubber lining.
Car	Starter motor, window motor, viper motor.
Computers	Disk drive, fan motor, speaker etc.
VCD and DVD	Main wheel motor.

1.11 Aim of the present work

Among the class of permanent magnets, barium ferrite permanent magnet is the cheapest with moderate magnetic properties. Extensive research has been carried out to study the effect of the various process parameters on the magnetic properties, microstructure and phase present. Various method which includes soild state method, chemical method, HEBM method has been adopted for making hexaferrites. In the mentioned processing method different precursors has been used. However, formation of hexaferrite from monoferrite has not been reported. In the present work, the main

motivation was to make the barium hexaferrite by barium monoferrite by using different molar ratios.

Chapter 2

Literature Review

Literature review

Since the discovery of the M-type hexagonal ferrites in 1950s, it has being of great interest due to its application as permanent magnetic materials and perpendicular recording media. The main reason for its great success is its low cost at moderate magnetic properties. Various work has been carried to develop hexaferrite by various methods and their properties has been investigated. On other hand extensive work has been done to understand the effect of various dopant for Ba and Fe. It is found the doping of metal ion, rare earth ion substantially effects their properties. Work carried out in past few year on different processing methods and different dopants are given below:

In 2000 Gonzalez-Carreno T, Morales MP, Serna CJ studied the nanoparticles of $BaFe_{12}O_{19}$ (10 nm in diameter) by combination of two methods, the citrate precursor and the aerosol pyrolysis technique [24]. The hexaferrite phase was found at lower temperatures at 1000 ^{0}C. The particle size was increased up to 100 nm in diameter by heat treatment at 1000 ^{0}C in an oven. The obtained particles are spherical aggregates of 400 nm, which can be easily disaggregated by grinding in a mortar. Saturation magnetization and coercivity values obtained for the largest particles were similar to those found for commercial Figments, 50emu/g and 5600 Oe, respectively.

In 2000 Ng WK, Ding J, Chow YY, Wang S, Shi Y prepared fine particles of barium ferrite with high coercivity (450kA/m) by chemical co-precipitation method [25]. Magnetic properties of the bonded barium ferrite magnet were measured at different temperatures. Mechanical milling was utilized to prepare ultrafine dispersed

barium ferrite particles. A weak anisotropy in the coercivity and remanence was found in the directions parallel and perpendicular to the compaction direction.

In 2001 Janasi SR *et. al*. produced barium ferrites by the ceramic method. Ferrite powders were obtained by co precipitation [26]. This method can produce high purity materials, i.e. particles composed of only Ba0.6Fe2O3. The effects of the pH during co precipitation and calcinations temperature in the magnetic properties were investigated. The molar ratio (Fe/Ba) used in this work was 10. The products were characterized by scanning electron microscopy and magnetic properties were evaluated by vibrating sample magnetometer. Particle size increases with decreasing pH and with increasing calcination temperature. Very fine particles were obtained. Intrinsic coercivities up to 4.80 kOe were achieved.

In 2010 Mohsen Q was study to synthesize stoichiometric and single phase barium hexaferrite by a technique of oxalate precursor. Effect of different annealing temperature on the particle size, microstructure and magnetic properties of the resulting barium hexaferrite powders has been studied [27]. The annealing temperature was in the range 800 to 1200 ^{0} C. The resultant powders were investigated by differential thermal analyzer (DTA), X-ray diffractometer (XRD), scanning electron microscopy (SEM) and vibrating sample magnetometer (VSM). Single phase of $BaFe_{12}O_{19}$ was obtained at annealing temperature 1200 ^{0}C. The SEM results showed that the grains were regular hexagonal platelets. Maximum saturation magnetization (66.36 emu/g) was observed at annealing temperature 1100 ^{0}C. However, it was found that the coercivity of the synthesized $BaFe_{12}O_{19}$ samples was lower than the theoretical values.

In 2005 A. Gonzalez-Angeles *et al.* successfully prepared the $Sn^{2+}Ru^{4+}$-substituted barium hexaferrite by mechanical alloying. It is found that Sn^{2+} –Ru^{4+} substitution is effective in maintains relatively high saturation magnetization (64.2 Am^2/kg), with easy control of the coercivity [28]. Increasing the substitution amount causes decrease in coercivity along with reduction of magnetocrystalline anisotropy. Mossbauer spectroscopy shows that the Sn^{2+} ions found on the octahedral sites (4f2 & 2a) sites, while the Ru^{4+} ions occupy the 4f1 & 2b sits.

Again in 2005 A. Gonzalez-Angeles *et al.* studies the effect of (Ni, Zn) Ru mixtures on magnetic properties of barium hexaferrites prepaired by high-energy ball milling [29]. It was found that the saturation magnetization (M_s) stays high ($66.5Am^2/kg$) and the intrinsic coercivity decreases rapidly, due to the high contribution to the anisotropy the cations are occupy to the $4f_2$ and 2b sites. The M_s valus of divalent cation reached high due to the magnetic nature of ZnRu mixture than of NiRu. It can be said that the Zn^{2+} is more effective to increase M_s than Ni^{2+}. Mossbauer spectroscopy studies showed that both ions mainly occupy the $4f_2$ and $2a+4f_1$ sites. The tetravalent Ru^{4+} ion has a special effect on magnetic properties of hexagonal ferrites (enhances M_s and decreases rapidly H_{ci} at low substitutions).

Ying Chen *et al* .studied the one-dimensional nonmaterial's synthesized using High-Energy Ball Milling and annealing process in 2006[30]. In this study, two different types of HEBM mills have been used: a vertical rotating ball mill and a planetary ball mill. The experimental results shows that HEBM has played an important role in the formation of the nanotubes and nanowires. HEBM creates a nanosized, disordered and more active structure in the precursor materials. The new

metastable structure has different properties than un-milled materials including large surface area, reduced vaporization temperatures and a lower activation energy. These new properties enable the growth of 1D structure possible during the low-temperature annealing process.

A. Ghasemi *et al.* again in 2006 analysis the electromagnetic properties and microwave absorbing characteristics of doped barium hexaferrite [31]. It was found that the ferrite grain size was almost depend on the chemical composition. The samples having higher magnetic susceptibility, higher permeability, larger coercive force and larger hysteresis loop shows the larger microwave-absorbing ability. Microwave absorbers for the applications over 15GHz, and with satisfactory reflection losses, could be obtained at a thickness of 1.8mm by controlling the substituted value of Mn, Cu and Ti elements in barium ferrite.

In 2007 G. Litsardakis *et al.* studied the structural and magnetic properties of barium hexaferrites with Gd–Co substitution by the conventional ceramic route [32]. Simultaneously substitution of b Gd for Ba and Co for Fe causes secondary phase formation which reduces magnetization value. A considerable increase in coercivity was found.

In 2007 P.Sharma *et al*, prepared two series of barium hexaferrites one by mechanical alloying and other by conventional route [33]. A reduction in phase formation temperature is found as compared to conventionally prepared powder. The higher amount of hexaferrites phase formed in the mechanically processed samples accounted for the higher M_S and M_R. The H_C enhancement in the mechanically

alloyed samples is attributed to its smaller particle size as compared to the conventionally prepared samples.

In 2007 M. Radwan *et al.* prepared barium hexaferrite nanoparticles by chemical coprecipitation [34]. The effect of Fe/Ba molar ratio was studied. Samples were calcined at different temperature. The addition of surfactants enhances the formation of single phase barium hexaferrite at low calcination temperature and helpful in controlling microstructure

In 2007 L. Lechevallier *et al.* studied the influence of the presence of Co on the rare-earth solubility in M-type hexaferrite [35]. The magnetic properties of strontium hexaferrites can be improved by the combined substitutionn of Pr and Nd. The results of XRD and Mossbauer spectrometry shows that the solubility of Pr and Nd atoms in M-type hexaferrites is higher in Co containing powders than in Co-free powders. Moreover, for the same composition, the solubility of Pr in the M-type phase is higher than that of Nd.

P Sharma *et al.* in 2008 studied the Structural, Mössbauer and magnetic studies on Mn-substituted barium hexaferrites prepared by high energy ball milling and thermal annealing [36]. The magnetization decreases with increasing the substitution amount due to the dilution of the magnetic structure. The increase in coercivity is due to the decrease in lattice parameter, c, which may enhance the super exchange interaction between neighboring ions.

In the same year 2009 Muhammad Javed Iqbal analyzed the effect of doping of Zr–Zn binary mixtures on structural, electrical and magnetic properties of Sr-hexaferrite nanoparticles of strontium hexaferrite doped with Zr–Zn are synthesized by a chemical co-precipitation method [37]. The crystallite sizes of 30–47 nm are small enough to obtain a suitable signal to noise ratio for application in the magnetic recording media. The temperature dependent DC resistivity of Zr–Zn doped samples shows metal-to-semiconductor transition in the temperature (*T*MS) range of 388–408 K. The Curie temperature, DC resistivity and activation energy for hopping decrease but the dielectric constant, dielectric loss and drift mobility increase by enhancing Zr–Zn content. With the substitution of Zr–Zn content of $x \leq 0.4$ the saturation magnetization, magnetic moment and remanence increase from 71 to 92 kAm−1, 11.2–13.6_B and 55–59 kAm−1, respectively, while coercivity decreases from137 to 34 kAm−1. With the improvement in the values of the above-mentioned parameters, the synthesized materials may be suitable for potential application in recording media.

The tailored magnetic properties of Sm(Zn) substituted nanocrystalline barium hexaferrites was studied by the Sha Jian *et al.* [38]. It was found that the doping greatly affects the phase composition and the magnetic properties. The substitution of Sm lead to the increase of M_s firstly, and then decreased, but H_c increased with doping. The magnatic properties indicate that the doped-Zn^{2+} substituted Fe^{3+} at $4f_2$ site.

In the recent years most work are done on the nanoparticles. Iftikhar Hussain Gul *et al.* studied the structural, magnetic and dielectric properties of Zr–Cd substituted strontium hexaferrite nanoparticles [39]. The saturation magnetization was found to

increase at low doping content of while the coercivity decrease for all the doped samples. The smaller crystallite size and increase in saturation magnetization while decrease in coercivity reveals that the synthesized materials are suitable for their applications in the recording media. The dielectric constant decreases with increasing frequency for all the samples. The decrease in dielectric constant has been explained on the basis of space charge polarization resulting from electron displacement and is a major contributor to the dielectric constant in ferrites.

S.A. Seyyed Ebrahimi studied the preparation of strontium hexaferrite nano-crystalline powder by carbon monoxide heat treatment and re-calcination from conventionally synthesized powder in 2009. First strontium hexaferrite was obtained by the conventional route with calcination of strontium carbonate and hematite at 1100 ^{O}C for 1h. Then strontium hexaferrite was isothermally subjected to carbon monoxide dynamic atmosphere at various temperatures and flows for different times [40]. Strontium hexaferrite decomposed into hematite and strontium oxide during the carbon monoxide heat treatment and the resultant iron oxide was then reduced by carbon monoxide mainly to metallic iron. This process made the microstructure much finer.

Muhammad Javed Iqbal, In the present work, $Sr_{0.5}Ba_{0.5}Fe_{12}O_{19}$ hexaferrite has been doped with a binary mixture of lanthanum and nickel using chemical co-precipitation method of synthesis [41]. The crystallite size of the synthesized samples is estimated in the range of 36–58nm and their structural analyses have confirmed a single magnetoplumbite phaseThe results shows the ferrimagnetic to paramagnetic transition at Curie temperature (TC) which deceases with the dopant content due to weakening of the super-exchange interactions. DC-electrical resistivity decreases with

increasing temperature showing the semiconductor like nature. High electrical resistivity combined with low dielectric constant and low dielectric loss.

Recently in the 2010 I. Bsoul *et al.* successfully investigate the Magnetic and structural properties of barium hexaferrite with its stoichiometric chemical formula $BaFe_{12}O_{19}$. In the present work concerned with the magnetic properties of BaM doped with gallium[42]. In this study they suggest that the preferential site occupation of Ga below this particular concentration is different than at higher concentration. The effect of Ga substitution for Fe results in an increase in the coercivity, which is attributed to the decrease of the magnetic exchange coupling. The reduction in exchange coupling is confirmed by the broadening of SFD and the decrease in remanence ratio and Curie temperature with increasing Ga concentration.

Yue Liu *et al.* investigated Co-Zn-Sn doped barium hexaferrites in the present year 2010 [43]. An increase in saturation magnetization (71.9emu/gm) has been achieved.

Chapter 3

Experimental Detail

Experimental detail

Overview

In this chapter the details of sample preparation including, weighing, mixing and various characterization techniques used to make the barium hexaferrite and inherent parameters are explained. The samples are prepared in bulk form via technique namely Solid State Reaction.

3.1 Sample preparation

In the present study the two kind of samples were prepared. Firstly the barium monoferrite was prepared then the barium hexaferrite was prepared using the as prepared barium monoferrite as one the component.

3.1.1 Preparation of barium monoferrite

The raw material used in the study were $BaCO_3$ (purity 99.0% Loba Chemicals) and Fe_2O_3 (Purity 99.0% Sigma-Aldrich grade) . The composition of the sample was taken according to reaction equation given below:

$$BaCO_3 + Fe_2O_3 \rightarrow BaFe_2O_4 + CO_2$$

The equimolar composition of $BaCO_3$ and Fe_2O_3 was weighed according to above formula and thoroughly premixed by using pestle and mortar for 30 minute. Further the mix were wet milled for three hours in a planetary ball mill. Zirconia jar and ball were used for the milling., The ball to charge ratio was 2:1 and rpm of the milling was fixed to 60. After milling, the excess acetone was drained and powder was dried in air over night. Further the powder were kept in alumina boat and calcined in air between the temperature range 800 to 1100 ^{0}C in tubular furnace. The heating cooling rate was fixed to 5 ^{0}C/minute and the holding time was 2 hours.

3.1.2 Preparation of barium hexaferrite

For the preparation of hexaferrite Fe_2O_3 (purity 99.0% Aldrich grade) $BaFe_2O_4$ was used. The powders were mixed in different Fe/Ba molar ratio. The compositions of the powders were takes according to the equation below.

$$BaFe_2O_4 + xFe_2O_3 \rightarrow BaFe_{12}O_{19}$$

Where x varies from 4.25 to 5.0 with the interval of 0.25. . The powder was weighed according to above formula. After weighing powder were mixed in pestle and mortar for 30 minute. The ball to charge ratio was 2:1 and homogenized in acetone media in zirconia zar using planetry ball milling for 3h with 60 rpm, then dried in air. The calcination of the samples were carried out in tubular furnace. The calcination temperature for all samples was 1150 ^{0}C and calcination time was 3 hour. The heating and cooling rate was 5 ^{0}C /minute for all the samples.

The chart given below shows the complete process for making barium monoferrite ($BaFe_2O_4$) and barium hexaferrite ($BaFe_{12}O_{19}$).

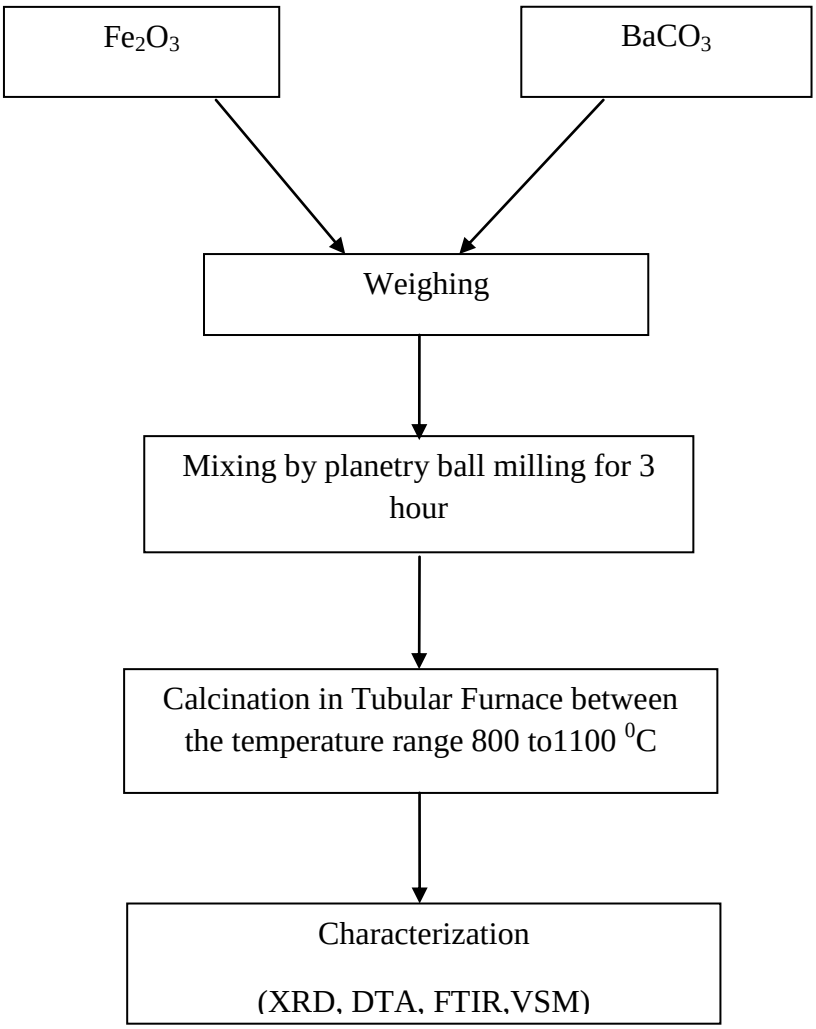

Figure3.1 Flow chart for making barium monoferrite

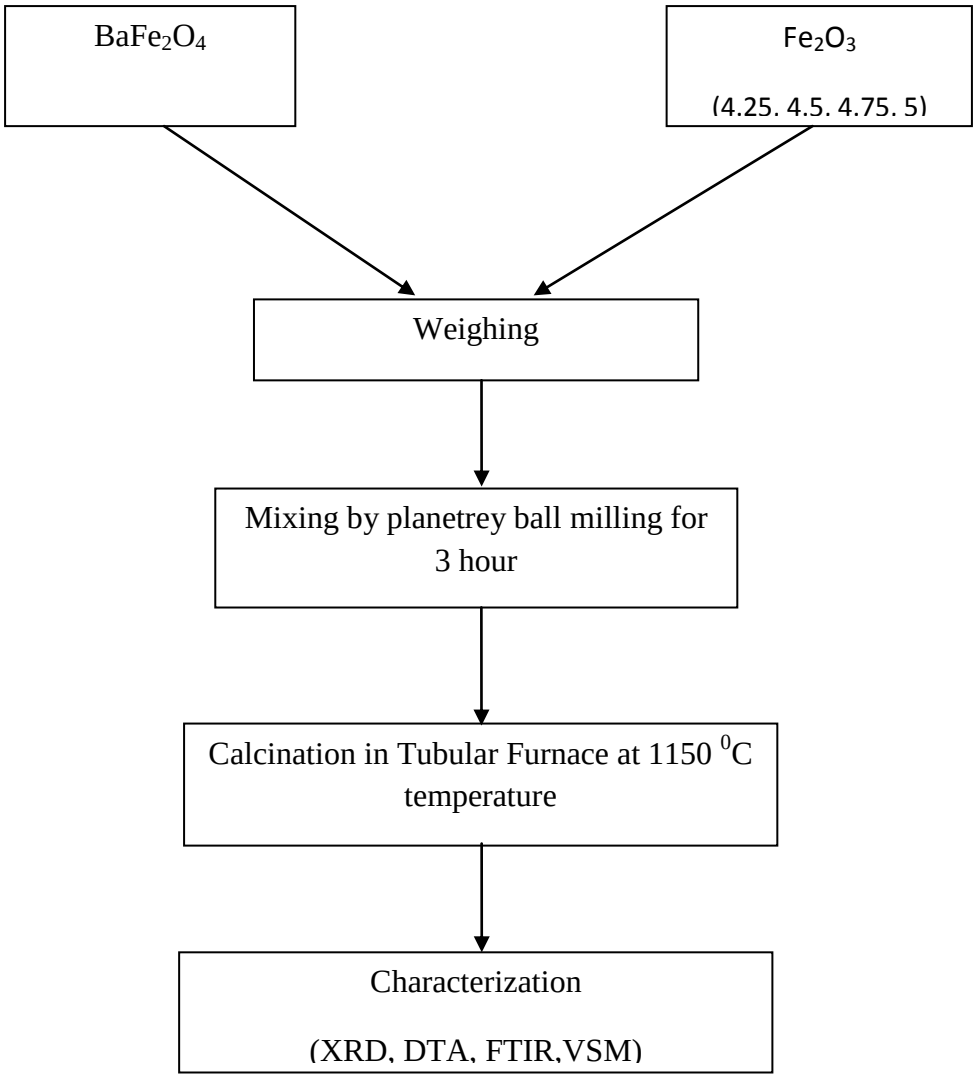

Figure3.2 Flow chart for making barium heaxferrite

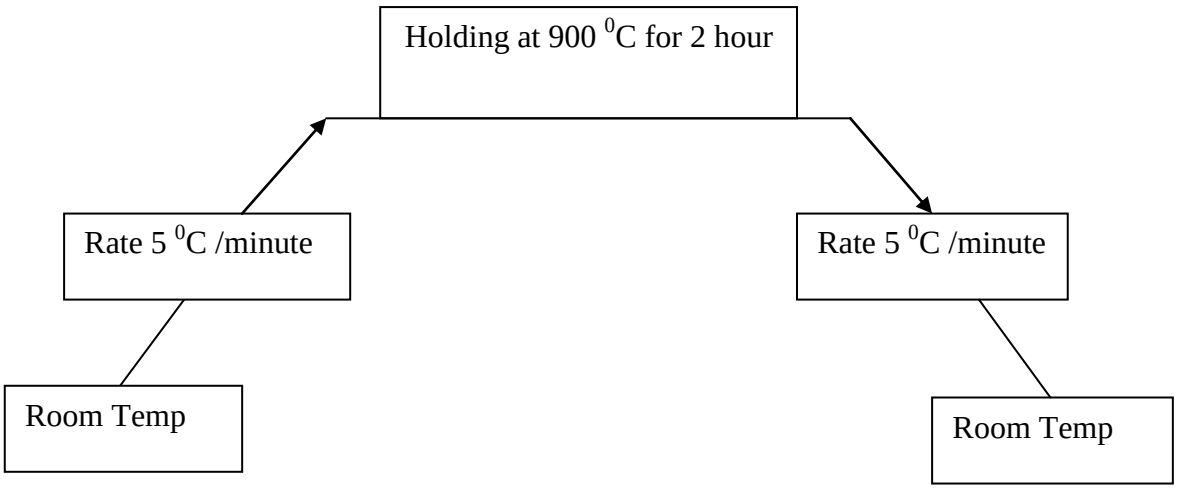

Figure 3.3 Calcination profile for barium monoferrite

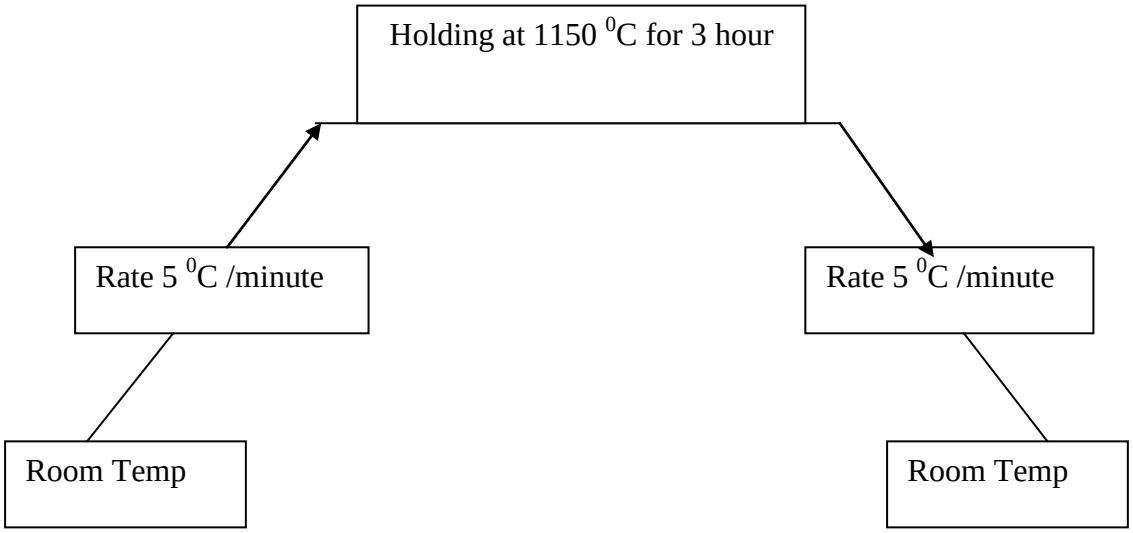

Figure 3.4 Calcination profile for barium hexaferrite

To understand the phase formation temperature thermal analysis was carried out by Differential Thermal analysis (DTA) model Perkin BTA/TGA and thermogravimetry analysis was done by the same model. The sample was run up to 900 ^{0}C with heating rate 10 ^{0}C/minute referring to thermal analysis result.

The phase identification of the calcined powder was carried out by X-ray difractometer, X'PERT Pro-Panalytical using Cukα radiation with λ=1.540Å. It was supplied by current intensity of 40 mA and voltage 45 kV.

The magnetic properties of the sample were measured by vibrating sample magnetometer (VSM) with a maximum applied field of 1.5kOe at room temperature.

Chapter 4

Results and discussion

Results and discussion

4.1 Characterization of raw materials

Figure 4.1 (a, b) shows the X-Ray diffraction pattern of pure $BaCO_3$ and Fe_2O_3 respectively. It is found that both are single phase. The sample present a single phase of $BaCO_3$ identified as orthorhombic structure according to index card JCPDS-441487.The XRD of Fe_2O_3 show the single phase identified as rhombohedral α-Fe_2O_3 structure according to index card JCPDS-890597. The crystallite size of $BaCO_3$ and Fe_2O_3 calculated by Debye Scherer formula [1]:

$$D = \frac{k\lambda}{\beta \cos \theta}$$

Where D is the crystallite size, k is the Scherer constant, λ is the wave length of radiation (λ=1.54Å), β is the peak width at half maximum measured in radian, and θ the peak angle. The crystallite size for pure $BaCO_3$ is in between the range 20nm to25nm and for pure Fe_2O_3 range from 30nm to35nm.

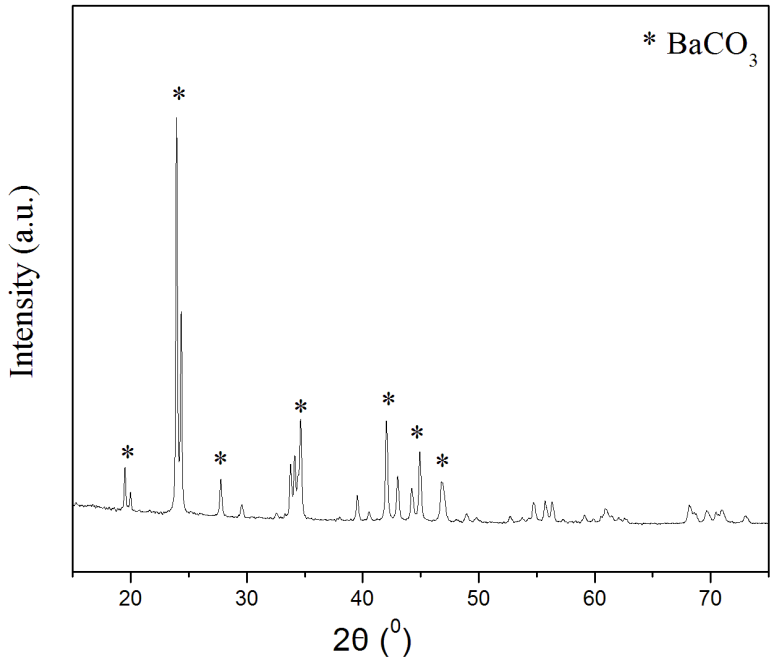

Figure 4.1(a) XRD pattern of pure $BaCO_3$ powder

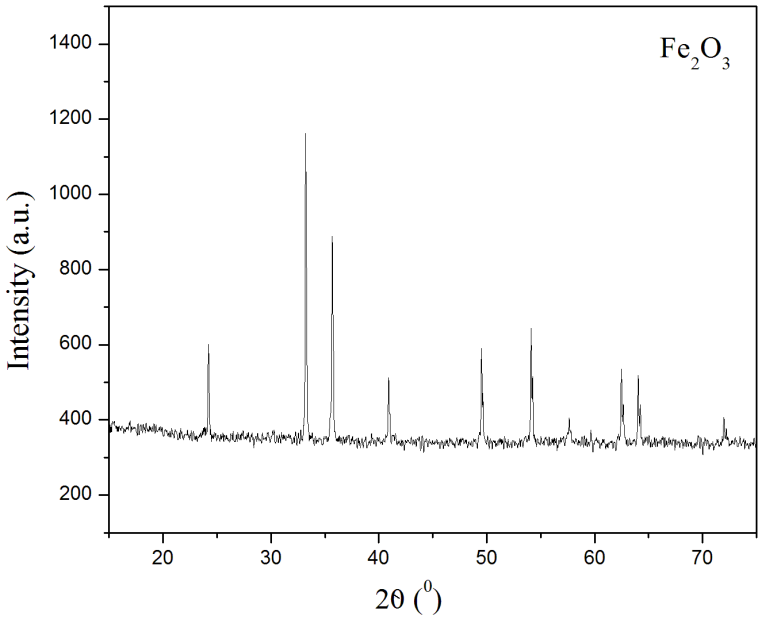

Figure 4.1(b) XRD pattern of pure Fe_2O_3 powder

4.2 Thermal analysis

All the powder is characterize before heat treatment as follows: the reaction temperature of powder were determine by differential thermal analysis (DTA). The figure 4.2 shows the DTA of mixed ($BaCO_3$ and Fe_2O_3) sample up to 900 ^{0}C. The heating rate was 10 ^{0}C/minute. Two peaks at 300 ^{0}C and 800 ^{0}C are observed. The exothermic peak at 300 ^{0}C is due to some moisture and endothermic peak at 800 ^{0}C shows phase the formation of barium monoferrite.

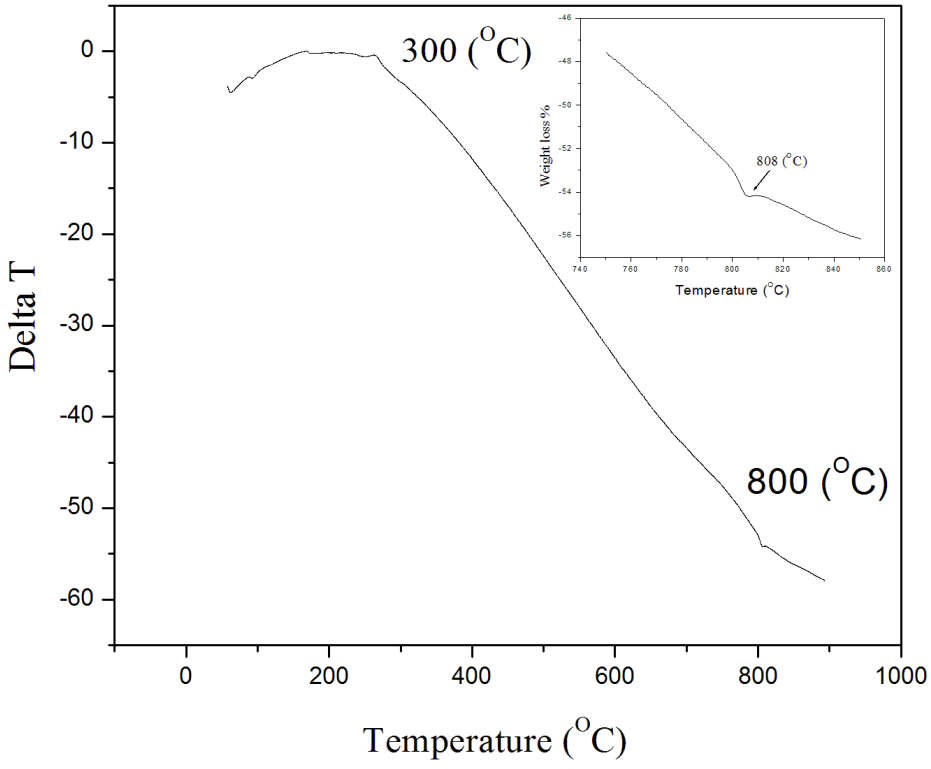

Figure 4.2 DTA graph of Fe_2O_3+$BaCO_3$ mix powders

Figure 4.3 shows the graph of TGA of mixing of $BaCO_3$ and Fe_2O_3 with the molar ratio is 1:1 and up to 900 ^{0}C with the rate of 10 ^{0}C/ minute. The sample runs in the

range between the 0 to 900 ^{0}C. The graph shows that, in the temperature range from 0 to 700 ^{0}C the weight of the sample seems to be almost constant but as the temperature further increase above the 700 ^{0}C, then we found that drastically weight loss. The weight loss decrease from 700 to 1000 ^{0}C. This suggest that monoferrite phase phase formation occurs at 700^{o}C.

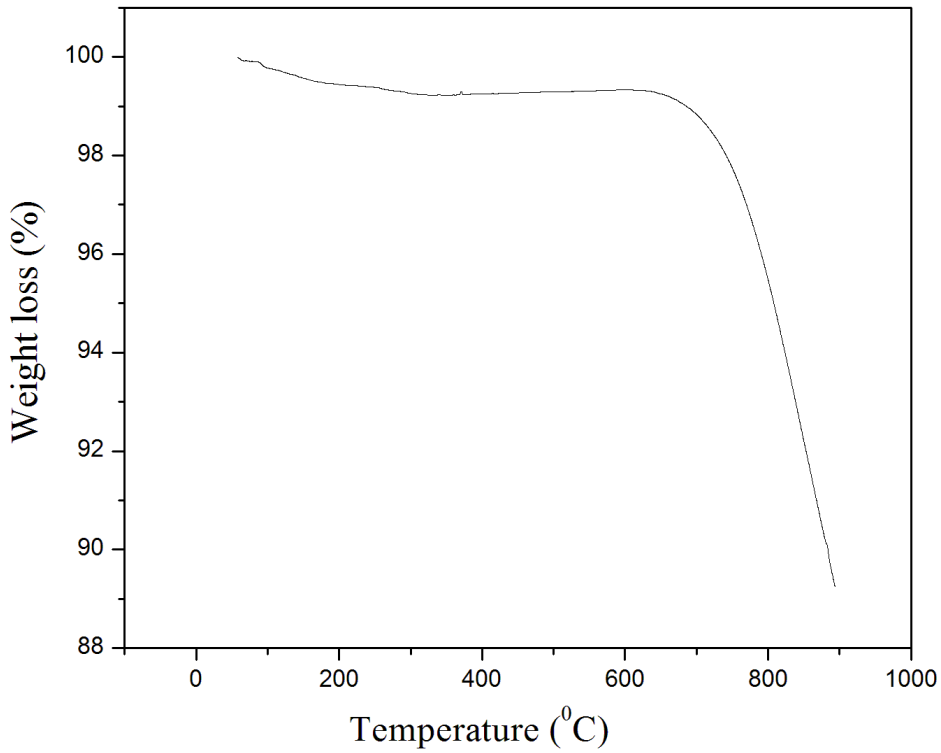

Figure 4.3 TGA graph of Fe_2O_3+$BaCO_3$ mix powders

The figure 4.4 shows the X-ray pattern of barium monoferrite calcined at different temperature range between 800 to1100 ^{0}C.

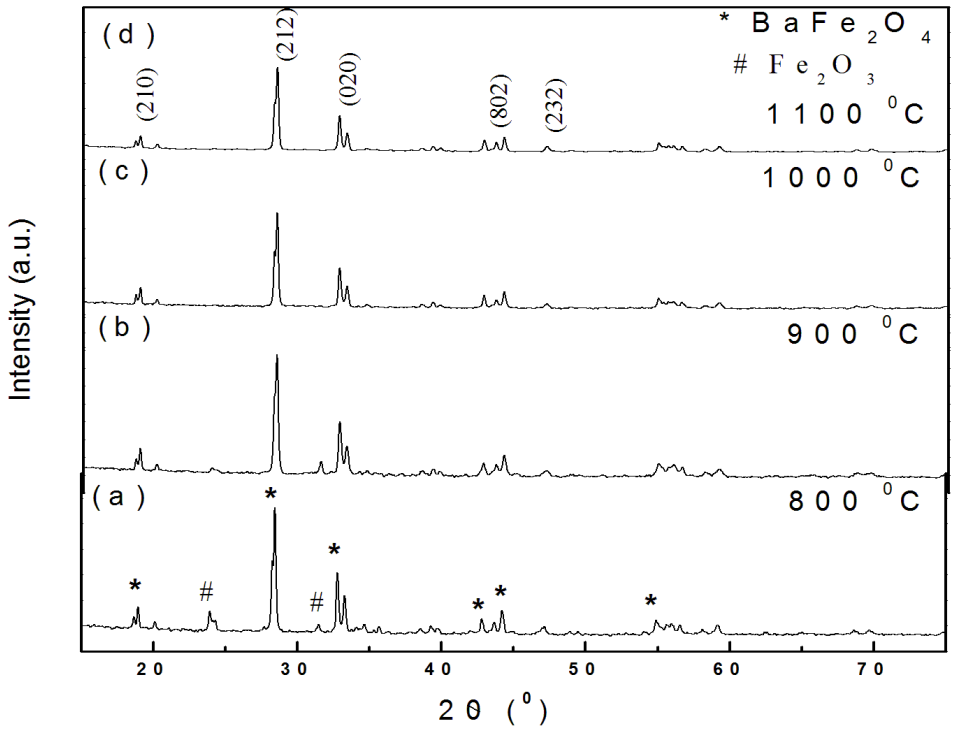

Figure 4.4 X-ray diffraction pattern of the barium monoferrite ($BaFe_2O_4$) Calcined at different temperatures (a) 800 ^{0}C (b) 900 ^{0}C (c)1000 ^{0}C (d) 1100 ^{0}C

After heat treatment at 800 ^{0}C, the XRD pattern shows the barium monoferrite phase as the major phase and with minor residual amount of Fe_2O_3. But after heating above 900 ^{0}C temperature the residual phase removed, only single phase barium monoferrite with orthorhombic spinel structure was found. The Xray were matched with JCPDS-460113 The crystallite size was measured by the Scherer formula given earlier.

At 800 ^{0}C highest crystal size is 27.80 nm but as increase the temperature the crystal size first decrease, than increase with temperature. The values of crystallite size measured are given in the table 4.1. Figure 4.3 show the variation of cryatllite size with temperature.

Table 4.1 Crystallite size of barium monoferrite at different temperature

S. No.	Temperature (^{0}C)	Crystal size (nm)
1	800 ^{0}C	27.80
2	900 ^{0}C	27.71
3	1000 ^{0}C	30.46
4	1100 ^{0}C	34.05

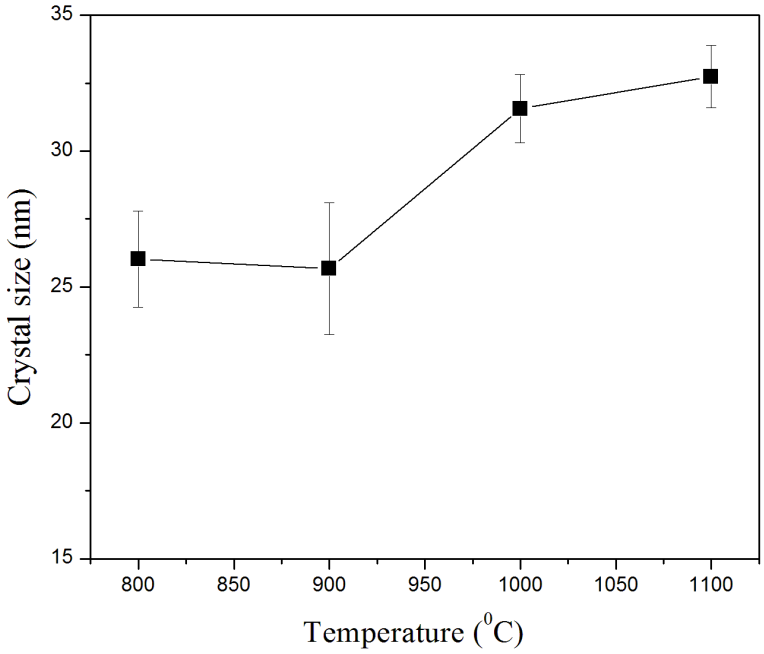

Figure 4.5 Variation in crystallite size of barium monoferrite with temperature

Figure 4.6 shows the DTA graph of $BaFe_2O_4 + 5Fe_2O_3$ powder upto 900^{o}C. The graph shows that, one exothermic peak at 300 ^{0}C temperature. After 300^{o}C there was no other peak is found. This suggest that the phase formation temperature is well above 900^{o}C. Keeping DTA results in mind the calcinations of the powders were selected to 1150^{o}C.

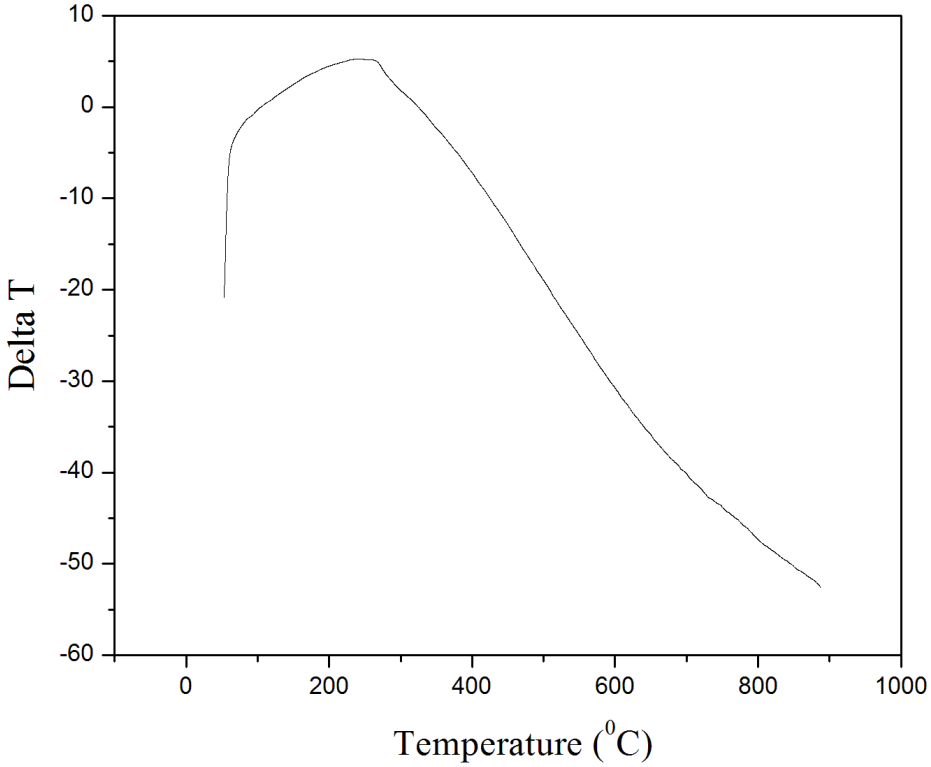

Figure 4.6 DTA graph of $BaFe_2O_4$ + $5Fe_2O_3$ mix powder

Figure 4.7 (a-d) shows the XRD pattern of barium hexaferrite with different Fe/Ba molar ratio calcined at 1150 ^{0}C. The XRD patterns were matched with index card JCPDS-430002. It was found that, at lower molar ratio upto 4.5 single phase hexaferrite is formed. With increase in molar ratio to 4.75 followed by 5.0 residual amount of Fe_2O_3 was present.

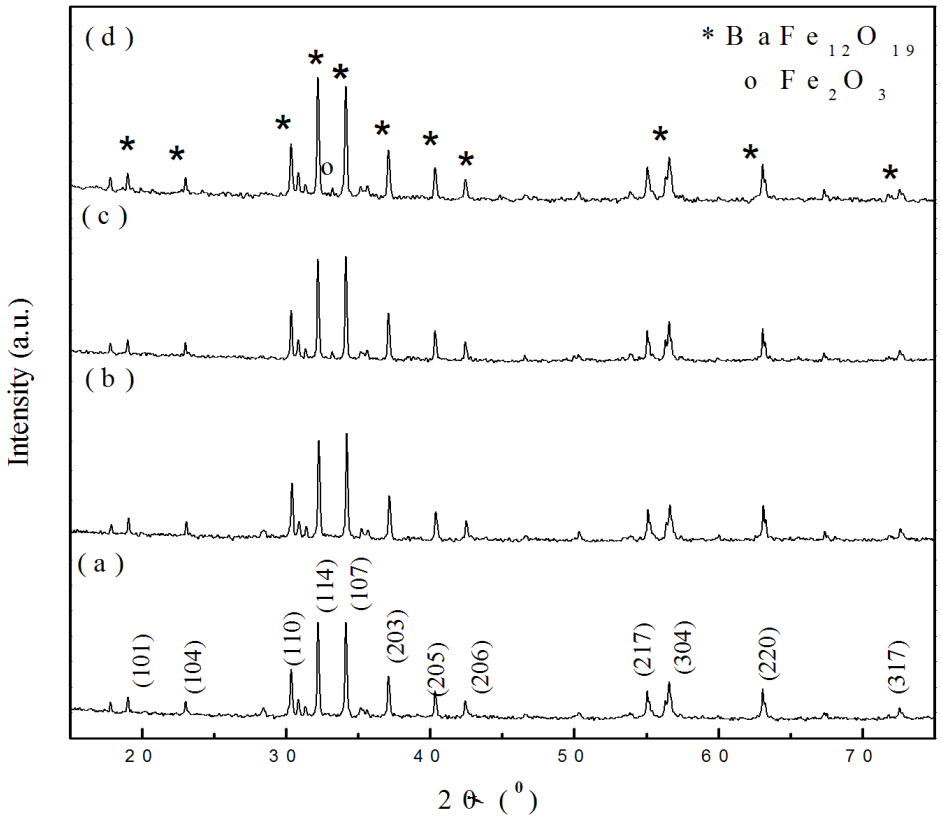

Figure.4.7 X-ray diffraction pattern of $BaFe_{12}O_{19}$ powder with different $BaFe_2O_4$: xFe_2O_3 molar ratio of Fe_2O_3 (a) x = 4.25, (b) x= 4 .5, (c) x = 4.75, (d) x= 5.0 calcined at 1150 ^{0}C

The crystallite size is measured by well-known Scherer formula given earlier. The crystal size of $BaFe_{12}O_{19}$ with different composition of Fe_2O_3, is given in table. It found that as increase the composition of Fe_2O_3, the particle size remain constant.

Table 4.2 Crystal size of barium hexaferrite (nm) with Composition of Fe_2O_3

S .No.	Composition of Fe_2O_3	Crystal size (nm)
1	4.25	33.58
2	4.5	33.58
3	4.75	33.58
4	5	33.58

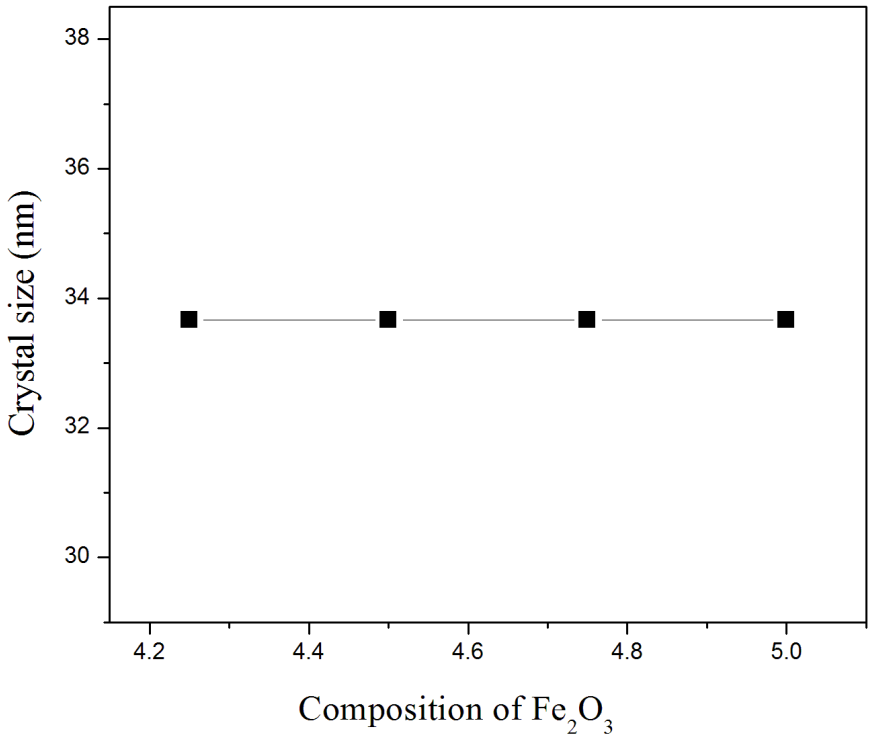

Figure 4.8 Variation of crystal size of barium hexaferrite with composition of Fe_2O_3

4.3 Magnetic characterization

Figure 4.9 shows the *RT* magnetization behaviour of BaFe2O4 samples calcined at 900^{o}C. The magnetization behaviour is similar to that of hard magnetic materials. The saturation magnetization at 10 kOe field is 1.5 emu/gm and coercivity is found to be 2.75 kOe.

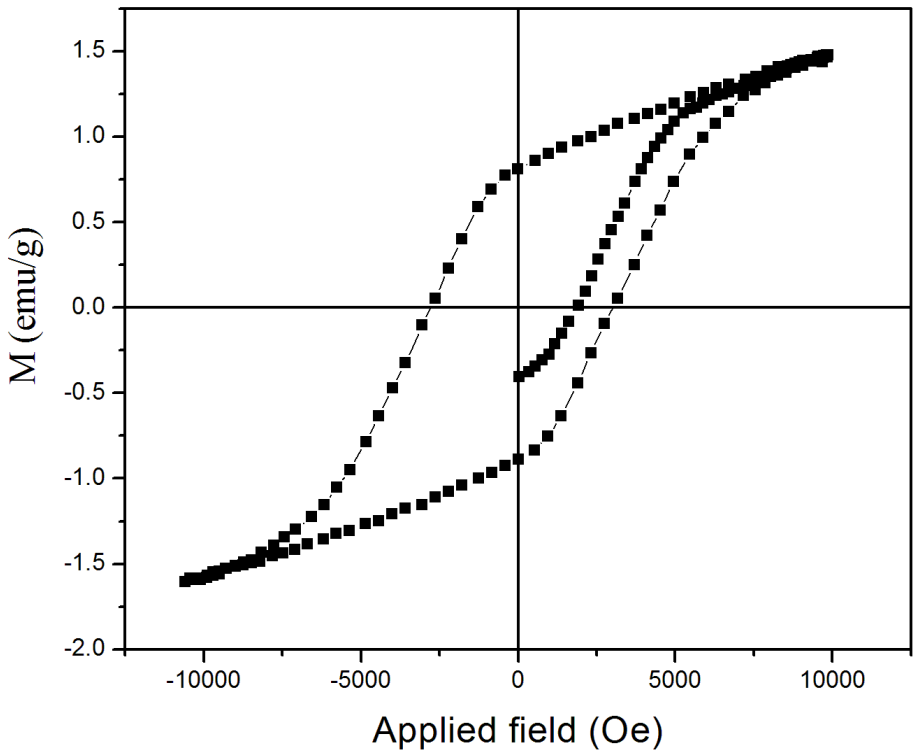

Figure 4.9 *M-H* behaviour of barium monoferrite

Figure 4.10 shows the magnetization behaviour of barium hexaferrite prepared by barium monoferrite at two different molar ratio.It is avident from the curve the saturation magnetization and coercivity increase with increasing Fe/Ba molar ratio.The saturation magnetization value increased from 46.8449 to 55.4803 for 4.5 to 5 molar ratio respectively.The coercivity of the sample is increase from -1161.6273 to

-3473.766 . Which show that low saturation magnetization in lower molar ratio sample may due to the vacant iron spin up site ,with increasing molar ratio the vacant iron site get filled and large saturation is achived.

On the other hand the hard magnetic properties are increased with increase in molar rat

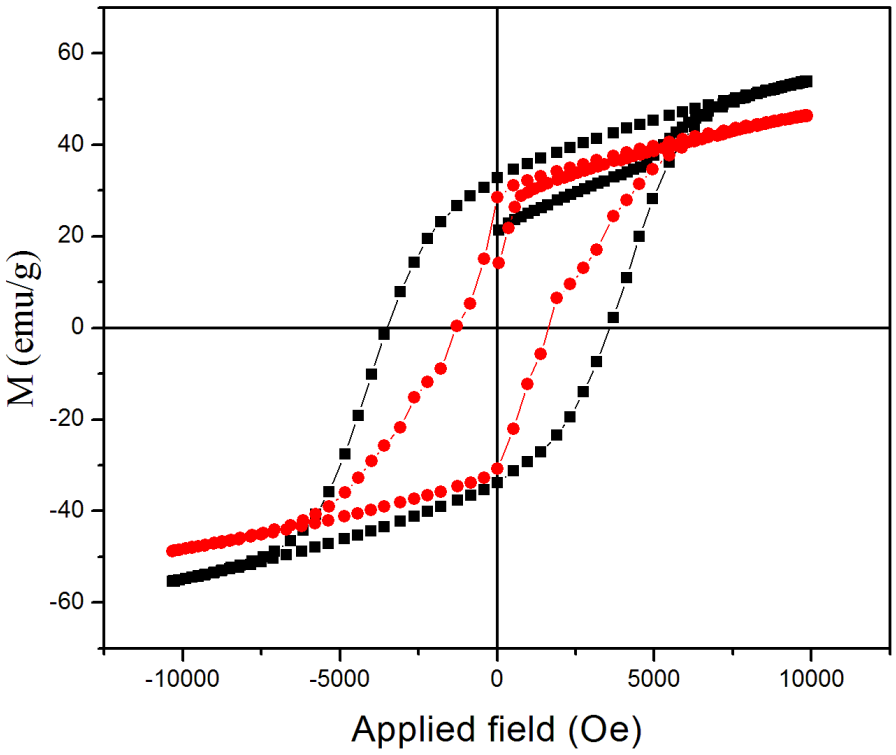

Figure 4.10 *M-H* behaviour of barium hexaferrite with 4.5 and 5 composition of Fe_2O_3

Chapter 5

Conclusion

Conclusion

The investigation was performed on $BaCO_3$ and Fe_2O_3 mixture, after 3 hour mixing and heat treatment in the temperature range 800 to 1100 ^{0}C. Above 900 ^{0}C temperature single phase of barium monoferrite was observed, with partical size in the range 30 to 35 nm by XRD pattern. All residual phases were removed above the 900 ^{0}C temperature. The annealing process cause increase content of hard magnetic barium monoferrite. The coercivity of barium monoferrite calcined at 900 ^{0}C was found 2.75KOe and saturation magnetization at 10 KOe field is 1.5emu/gm.

After this for making barium hexaferrite, $BaFe_2O_4$ and Fe_2O_3 was used as raw material and calcined the mixture of $BaFe_2O_4$ and Fe_2O_3 at 1150 ^{0}C with different composition of Fe_2O_3. The X-ray differection patteren identified the $BaFe_{12}O_{19}$ and Fe_2O_3 calcined at 1150 ^{0}C with composition $5Fe_2O_3$.But after decrease the composition of Fe_2O_3 (4.5) then. Only single phase of barium hexaferrite was obtained with partical size 30 nm. It has hexagonal structure. The saturation magnetization and coercivity of barium hexaferrite increase with increasing Fe/Ba molar ratio. The saturation magnetization value increased from 46.8449 to 55.4803 for 4.5 to 5 molar ratio. Coercivity of the sample increased from -1161.627 to -3473.766. The hard magnetc properties increased with increase the molar ratio.

References

[1] W. Ervens and H. Wilmesmeier, Ullmann's Encyclopedia of Industrial Chemistry, fifth editionA16 (1990), 1-51.

[2] C.W. chen, Magnetism and Metallurgy of Magnetic materials, North Holland Publshing Company, 1997.

[3] W.H. Yeadon & A. W. Yeadon, Handbook of small Electric Motors, Mcgraw Hill Company Inc. USA, 2001.

[4] M. V. Rane, D. Bahadur, S. D. Kulkarni & S. K. Date, J. Magn, Magnetic Material 293 (1999), 1256.

[5] S. Hirosawa, A. Hanaki, H. Tomizawa and A.Hamamur, Physica B, vol. 164,(1990), 117-123.

[6] J.D. Livingston, "A review of coercivity mechanisms", J. Appl. Phys. (1981), 522-541.

[7] Min Chen and David E. Nikles, Nano Lett. (2002) 211–214.

[8] F.X.N.M Kools and D. Stoppels, Kirk-Othmer Encyclopedia of Chem. Tech., Fourth Edition10, (1993), 381-413.

[9] Carter, C. Barry; Norton, M. Grant, Springer, 2007 ISBN 0387462708.

[10] Shriver, D. F.; Atkins, P. W.; Overton, T. L.; Rourke, J. P.; Weller, M. T.Armstrong.

[11] E.W. Gorter, 1957, Proceeding IEEE, 104B, (1957), 2255-2257.

[12] V. Adelskold, Arkiv. Kemi. Min. Geol., 12A, (1938), 1-4.

[13] P.B. Braun, Philips Res. Rep, 12, (1957), 491-494.

[14] P.W. Anderson, Physical Review, 79, (1957), 350-353.

[15] Y. Goto and K. Takahashi, J. of Jap. Soc. Powder Metallurgy, 17, (1971), 193- 197.

[16] F. Kamamaru, M. Shimada and M. Koizumi, J. Phy. Chem. Sol., 33, (1972),

[17] www.shibang-china.com

[18] Patnaik, P. Dean's Analytical Chemistry Handbook, 2nd ed. McGraw-Hill, 2004.

[19] Harvey, D. Modern Analytical Chemistry. McGraw-Hill, 2000.

[20] A.H. Lu, E.L. Salabas and F. Schüth, Angew. Chem., Int. Ed., 2007, 1222-1244

[21] Brinker,C.J., G.W. Scherer, Academic Press. (1990), ISBN 0121349705.

[22] Hench, L.L., J.K. West, Chemical Reviews (1990).

[23] J. Beretka and M. Ridge, J. Chemical Society (A), (1968), 2463-2465.

[24] Gonzalez-Carreno T, Morales MP, Serna CJ, materials letters 43 (2000), 97-101.

[25] N.W.K, Ding J, Chow YY, Wang S, Shi Y, journal of materials research 15 (2000),2151-2156.

[26] Janasi SR, Rodrigues D, Landgraf FJG, Emura M, advanced powder technology 189-1 (2001), 661-666.

[27] Mohsen Q, journal of alloys and compounds 500 (2010), 125-128.

[28] A. Gonza´ lez-Angeles, G. Mendoza-Sua´ reza, A. Gruskova´ b, J. Lipkac, M.

[29] Papa´nova´ b, J. Sla´mad, Journal of Magnetism and Magnetic Material 285,(2005), 450–455.

[30] A.Gonza´lez-Angelesa,T, G.Mendoza-Suareza G.Mendoza-Suarez, A. Gruskova,

[31] J. Slama, J. Lipka, M. Papanova, Materials Letters 59 (2005), 1815–181.

[32] Ying Chen, Chi Pui Li, Hua Chen, Yongjun Chen, Science and Technology of Advanced Materials 7 (2006), 839–846.

[33] A. Ghasemi, A. Hossienpourb, A. Morisakod, A. Saatchia, M. Salehia, Journal of Magnetism and Magnetic Materials 302 (2006), 435.

[34] G. Litsardakis, I. Manolakis, K. Efthimiadis, Journal of Alloys and Compounds 427 (2007), 194–198.

[35] P. Sharma, R.A. Rocha, S.N. de Medeiros, A. Paesano Jr, Journal of Alloys and Compounds 443 (2007), 37–42.

[36] M. Radwan, M.M. Rashad, M.M. Hessien, Journal of Materials Processing Technology 181 (2007), 106–109.

[37] L.Lechevallier, J.M. Le Bretona, A. Morelb, P. Tenaudb, Journal of Magnetism and Magnetic Materials 316 (2007), 109–111.

[38] Puneet Sharma , R. A. Rocha, S. N. de Medeiros & A. Paesano Jr & B. Hallouche Journal of Alloys and Compounds 478 (2009), 736–740.

[39] Muhammad Javed Iqbal, Muhammad Naeem Ashiq, Pablo Hernandez Gomez, Journal of Alloys and Compounds 478 (2009), 736–740.

[40] Han Yanbing, Sha Jian, Sun Lina, Tang Quan, Lu Qin, Jin Hongxiao, Jin Dingfeng, Bo hong, Ge Hongliang,Wang Xinqing, Journal of Alloys and Compounds 48 (2009), 348–351.

[41] Iftikhar Hussain Gul, Muhammad Naeem Ashiqa, Muhammad Javed Iqbal,Journal of Alloys and Compounds 487 (2009), 341–345.

[42] A. Yourdkhani, S.A. Seyyed Ebrahimi, H.R. KoohdarS, Journal of Alloys and Compounds 470 (2009), 561–564.

[43] Muhammad Javed Iqbal, Saima Farooq, Materials Chemistry and Physics 118 (2009), 308–313.

[44] I.Bsoul, S.H. Mahmoob, Journal of Alloys and Compounds 489 (2010), 110–114.

[45] Yue Liu, MichaelG.B.Drew b, YueLiu a,n, JingpingWangc, MilinZhang, Journal of Magnetism and Magnetic Materials 322 (2010), 814–818.

[46] Bsoul, S.H. Mahmood, Journal of Alloys and Compounds 489 (2010), 110–114

.